Journal of
Nuclear Engineering

MDPI

Article

Intracore Natural Circulation Study in the High Temperature Test Facility

Izabela Gutowska [1,*], Robert Kile [2,3], Brian G. Woods [1] and Nicholas R. Brown [3]

[1] Radiation Center 100, School of Nuclear Science and Engineering, Oregon State University, Corvallis, OR 97331, USA
[2] Idaho National Laboratory, 1955 N. Fremont Ave, Idaho Falls, ID 83415, USA
[3] Zeanah Engineering Complex, Department of Nuclear Engineering, University of Tennessee, Knoxville, 863 Neyland Dr., Knoxville, TN 37996, USA
* Correspondence: izabela.gutowska@oregonstate.edu

Abstract: The development of the Modular High-Temperature Gas-Cooled Reactor is a significant milestone in advanced nuclear reactor technology. One of the concerns for the reactor's safe operation is the effects of a loss-of-flow accident (LOFA) where the coolant circulators are tripped, and forced coolant flow through the core is lost. Depending on the steam generator placement, loop or intracore natural circulation develops to help transfer heat from the core to the reactor cavity, cooling system. This paper investigates the fundamental physical phenomena associated with intracore coolant natural circulation flow in a one-sixth Computational Fluid Dynamics (CFD) model of the Oregon State University High Temperature Test Facility (OSU HTTF) following a loss-of-flow accident transient. This study employs conjugate heat transfer and steady-state flow along with an SST k-ω turbulence model to characterize the phenomenon of core channel-to-channel natural convection. Previous studies have revealed the importance of complex flow distribution in the inlet and outlet plenums with the potential to generate hot coolant jets. For this reason, complete upper and lower plenum volumes are included in the analyzed computational domain. CFD results also include parametric studies performed for a mesh sensitivity analysis, generated using the STAR-CCM+ software. The resulting channel axial velocities and flow directions support the test facility scaling analysis and similarity group distortions calculation.

Keywords: HTTF; VHTR; PCC; CFD; natural circulation

Citation: Gutowska, I.; Kile, R.; Woods, B.G.; Brown, N.R. Intracore Natural Circulation Study in the High Temperature Test Facility. *J. Nucl. Eng.* **2024**, *5*, 500–517. https://doi.org/10.3390/jne5040031

Academic Editor: Dan Gabriel Cacuci

Received: 30 April 2024
Revised: 10 September 2024
Accepted: 6 November 2024
Published: 14 November 2024

1. Introduction

Oregon State University, under the auspices of Idaho National Laboratory, assembled an integral test facility, the High Temperature Test Facility (HTTF), that delivers experimental data to validate thermal hydraulic system codes [1]. These codes, such as RELAP5-3D, are expected to simulate the scope of phenomena identified in the phenomena identification and ranking table prepared for the very-high-temperature reactor (VHTR) [2]. The facility is configured to test a variety of postulated depressurized conduction cooldown (DCC) and pressurized conduction cooldown (PCC) accidents as well as normal system operation.

During the PCC event, forced convection is lost, but the pressure boundary remains intact, eliminating any depressurization of the system or gas ingress into the vessel. Several phenomena can become important after the initiation of the PCC event. For instance, it is likely that localized natural circulation patterns will significantly affect the heat transfer to various parts of the vessel and structural materials in the system. These localized phenomena can include the mixing of hot gas jets exiting the top of the core or intracore, intrasystem natural circulation flow paths.

During normal operation, helium is driven downward through the core coolant channels by forced convection (Figure 1A). With the initiation of the PCC event, forced convection will cease. Inertial forces will continue to drive the gas flow in the downward

direction until friction and flow resistance slow the gas flow enough that gravity effects become important. At this stage, it is conceived that the gas flow in the coolant channels will reverse direction and begin to flow upward through the core as a result of the buoyancy caused by heating. The helium may undergo significant expansion in the core region due to local heating. The hot helium continues upward through the upper reflector into the upper plenum, where thermal radiation heat transfer from the vessel head cools the hot gas. The cooler gas then flows downward through the cooler channels. Then, cool helium enters the lower plenum and flows up through the core where it is heated. Mixing of these flows will take place in the lower and upper plenums. The chimney effect in the PCC event increases the core (and vessel) temperatures near the top [2]. A detailed model is needed to capture the elements of the core geometry and predict the temperature response at the smallest scale [3,4].

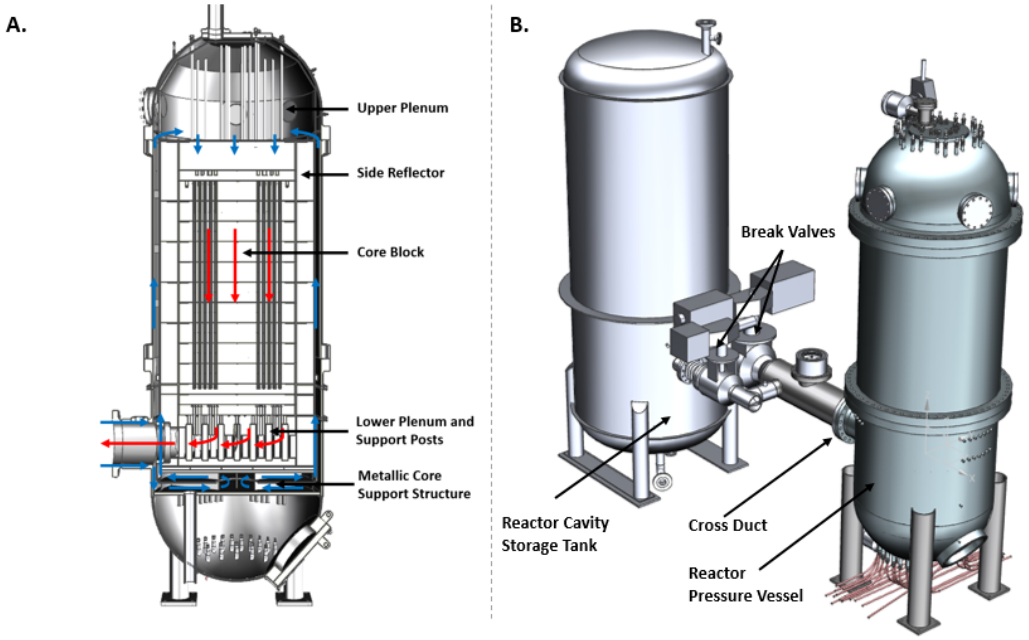

Figure 1. (**A**) Section view of the HTTF RPV and helium flow path; (**B**) HTTF system CAD model [1].

MacDonald [5] evaluated system performance needs under PCC conditions and stated that the core heat transfer is instrumental in setting the maximum temperature levels for fuel and materials research and development. The core heat transfer determines the material selection and configuration in the VHTR core and RCCS (Reactor Cavity Cooling System) designs. According to Vilim et al. [6], the main safety criteria are that the maximum fuel temperature should not exceed 1600 °C, and the maximum SA 508 or SA 533 vessel temperature should not exceed 425 °C during the PCC event. Further, MacDonald [5] underlined the need for computational fluid dynamics (CFD) validation calculations of prismatic reactors during a conduction cooldown event and the requirement for the experimental database to support validation activities. The ASME V&V 20-2009 defines validation as the determination of how closely a computational model corresponds to the physical reality. Before computational results are validated, the model implementation should be verified against the conceptual model to ensure numerical accuracy (model verification) [7].

Several CFD studies have analyzed the flow and heat transfer in the parallel heated channels geometry representative of the prismatic VHTR reactor during PCC and DCC scenarios. Tung et al. [8] performed a CFD analysis of natural circulation in the VHTR after a PCC, including grid and temporal convergence and partial validation studies. The CFD model comprised one-twelfth of a VHTR core, and upper and lower plenum volumes were represented by open regions. Oh et al. [9] investigated natural circulation patterns in the VHTR air-ingress scenarios using FLUENT. Their work focused on the DCC transient.

Another study of natural circulation was conducted by Tung and Johnson [10] for a single one-twelfth sector of a VHTR core block. Furthermore, the flow characteristics of the upper plenum jets impingement during the PCC transient were numerically investigated by Hassan [11]. Alwafi et al. [12] experimentally investigated the flow characteristics of a single isothermal water jet discharging into the upper plenum of a one-sixteenth-scaled facility of high-temperature gas-cooled reactors. Gutowska et al. [13] performed a CFD study of the HTTF PCC experiment using reference pretest full power conditions. That paper included detailed natural convection flow patterns, but the boundary and assumed test conditions were not indicative of the experiment executed after these simulations were performed. Nevertheless, that study forms a foundation for the work described in this paper.

This paper investigates local flow patterns during intracore natural circulation following the PCC using the detailed geometry of the HTTF core internals and boundary conditions derived from the RELAP5-3D model (built with reference to the HTTF experimental conditions). The PCC natural convection recirculation that follows nonuniform heating and results from asymmetrical core radial power profile, as these conditions reflect the *PG-27 Low Power (<350 kW) Complete Loss of Flow (2 heaters)* test experimental conditions, were studied (described in Section 4). This study resulted in a flow map of channels reversing the flow. The channel-to-channel axial velocity flow map can support test facility scaling analyses and similarity group distortions calculations. According to Woods [14], a similar distribution of channels in the upflow should be maintained between the integral test facility and reference reactor design to replicate PCC intracore flow behavior adequately. Lower and upper plenum and core temperature profiles were also extracted from this study. Finally, following the solution verification, the paper presents the effects of the HTTF reactor pressure vessel (RPV) internal structures on the free convection flow pattern. These results are compared with the symmetrical power profile assumption that was made in the previous PCC study performed by Gutowska et al. [13].

2. High Temperature Test Facility

The High Temperature Test Facility (HTTF) (Figure 1B) is a scaled-down representation (1:4 scale in both height and diameter) of the General Atomics Modular High-Temperature Gas-cooled Reactor (MHTGR) design. This facility is engineered to simulate conditions at temperatures comparable to those during a loss-of-forced-circulation event. The temperature scaling is maintained at a 1:1 ratio, with a maximum operating temperature reaching 1400 °C. It operates at a pressure scale of 1:8, with a maximum pressure of 0.8 MPa. Helium serves as the primary working fluid, while nitrogen is employed to simulate break scenarios.

The HTTF does not rely on nuclear fuel for power generation. Instead, it features an array of electrically heated graphite rods (graphite grade G-348), generating a thermal output of roughly 2.2 MWth, equivalent to 1:160 of the MHTGR's output. The system comprises 210 heater rods organized into 10 banks, each with three legs, and each leg contains seven heater rods.

To replicate the thermal behavior of the MHTGR's graphite prismatic block structure, ceramic blocks are used within the HTTF. These blocks, made of Greencast 94-F (96.5% alumina), form a core composed of 10 hexagonal units. The core is enclosed by reflectors on multiple sides, including two upper, three lower, and several lateral reflectors. The side reflectors are crafted from ShotTech SiC 80 (78% silicon carbide, 10.5% silica, and 8.3% alumina), while the top and bottom reflectors use Greencast 94-F. The design also incorporates three distinct sections simulating the core exit chamber: the lower plenum roof, the lower plenum housing 163 support posts, and the lower plenum floor. Figure 2A presents the cross-sectional view of the HTTF core block, showing 516 coolant channels and 210 heater channels, color-coded for clarity—blue, green, or yellow for coolant channels and red for heater rod voids. To manage core bypass flow, a graphite plate atop the upper reflector directs flow through designated inner and outer bypass channels.

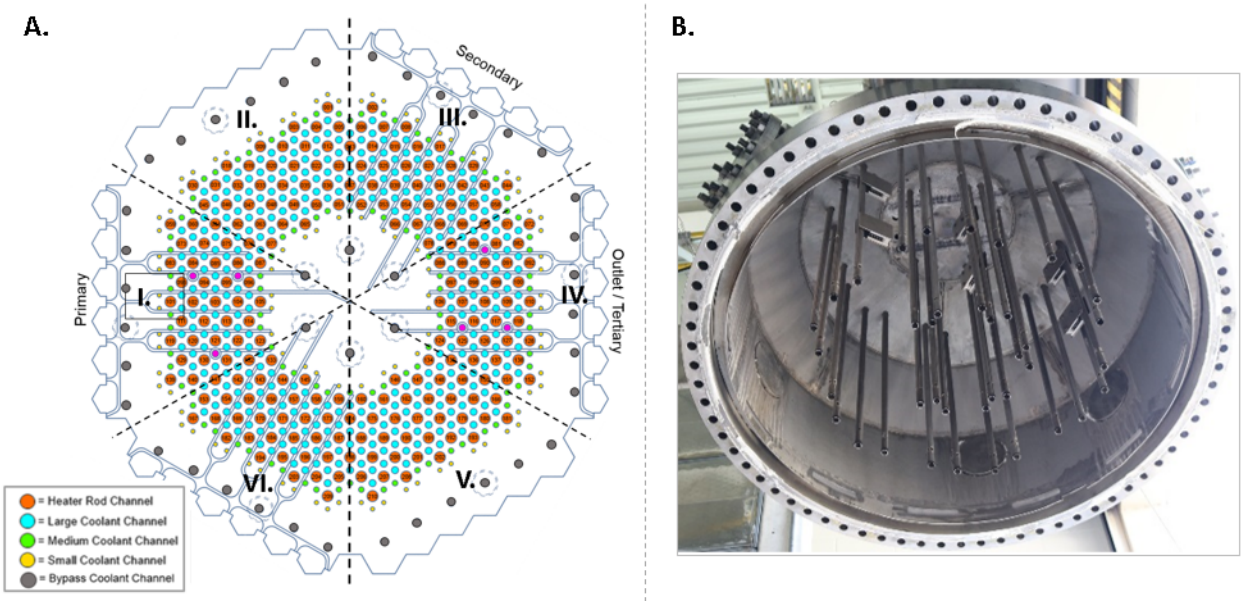

Figure 2. (**A**) Arrangement of coolant channels, bypass channels, and heater rods channels in the HTTF core block; (**B**) HTTF upper head with instrumented guide tubes [1].

Instrumentation within the HTTF is focused on primary, secondary, and tertiary core sections. The inlet plenum shroud (Figure 2B) contains 39 guide tubes accommodating thermocouples and gas capacitance sensors. In total, 42 thermocouples and six gas capacitance sensors are installed in the upper head region.

3. Pressurized Conduction Cooldown

During the PCC event, the cessation of forced coolant circulation leads to the initiation of natural circulation within the reactor system. The MHTGR's design features a heat sink, specifically the steam generator, positioned at a lower elevation compared to the core, which promotes the expected intracore natural circulation. As the coolant gas ascends from the core's hottest region, it enters the upper plenum, where it releases heat to the shroud before descending through the cooler core areas, eventually returning to the heated section. This circulation is driven by buoyancy forces arising from density variations caused by the decay heat from the differentially heated channels and the heat sink, which consists of the upper plenum and core channels. Collectively, these elements form a closed multichannel thermosiphon loop that allows for continuous coolant circulation.

Natural circulation through multiple parallel vertical channels with varying heat inputs is inherently complex, as the flow rate and direction are influenced by the thermal history of each channel's heat input. Safety assessments for gas-cooled reactors would greatly benefit from data on the onset of mixed convection and predictions regarding flow instability thresholds. To facilitate an understanding of the primary physical phenomena and the system's operating characteristics, the sequence of events following the PCC in the MHTGR can be categorized into three distinct phases based on the evolving flow conditions:

1. Circulator rundown—cessation of forced circulation;
2. The onset of natural circulation and flow reversal;
3. Quasi-steady-state multichannel thermosyphoning within the core volume.

This paper focuses on Phase 3 of the PCC transient.

4. HTTF PG-27 and RELAP5-3D Model

The HTTF *PG-27 Low Power (<350 kW) Complete Loss of Flow* experiment was conducted in April 2019. Unlike the sequence of events anticipated in the MHTGR during a similar scenario, the HTTF's conditions deviate in key aspects. Specifically, while the MHTGR's

circulator would undergo a gradual coast-down, the HTTF's setup results in the cessation of forced convection almost immediately, causing a rapid stagnation of flow. Moreover, in the HTTF, the steam generator thermal center is placed above the core thermal center; therefore, to establish the desirable initial conditions for the transient, the cold valve on the secondary side of the steam generator was closed during the test (a valve directing the secondary side coolant to the steam generator). This way, the steam generator was no longer serving the role of a system heat sink, the loop's natural convection flow was limited, and the intracore natural convection (as in the MHTGR) was enabled. The test's desired and initial conditions are shown in Table 1. The desired conditions are the conditions specified in the test procedure, while initial conditions were the conditions achieved and executed during the test. The loss of flow conditions and the associated decay curve were followed only during the first 4 h of the transient before the heating system tripped. Temperature readings collected during these 4 h do not clearly indicate the establishment of the intracore natural convection. The facility has no velocity measurements to help investigate the natural convection patterns. The RELAP5-3D model was built to help investigate the facility's transient behavior and long-term conditions following the PCC initiation.

Table 1. PG-27 test initial conditions.

Property/Component	Desired Condition	Test Initial Condition [1]
Temperature difference across the core (Outlet–Inlet)	567 °C	567 °C
Primary loop pressure	>130 kPa helium	206.72 kPa
RCCS pressure	>101 kPa helium	195.87 kPa
Cooling water system	Filled with water at ambient pressure	20.9 °C, 101.3 kPa
Steam generator fill up level	Between 60% and 80%	76%
RCCS tank	Filled with water at ambient pressure	20.9 °C, 101.3 kPa

[1] Temperature readings uncertainty of 4.284 °C; pressure readings uncertainty of 0.016 MPa.

The RELAP5-3D HTTF model we used in this work descends from the model described in reference [15]. Axial and radial nodalizations can be seen in Figure 3, where control volume numbers indicate component numbers in the model. The RELAP5-3D model represents the core as a set of three rings, each consisting of a flow channel, a heat structure for the core block, and a heat structure for the heater rods. These rings are components 140, 145, and 150 in Figure 3. The flow channels in the inner and outer reflectors are each also represented as a ring, but those rings do not contain heat structures for heater rods. Those are components 132 and 162, respectively. Components 164 and 166 represent gaps between the outer reflector and the permanent reflector (164) and the permanent reflector and the core barrel (166). Gaps are regions with stagnant helium that are not connected to the top plenum. The representation in Figure 3A shows the different types of channels, namely the inner reflector, core, outer reflector, and gap, as separate columns, but there are five total flow channels (132, 140, 145, 150, and 162). The RCCS is nodalized to match the nodalization of the reactor vessel. Channels are slightly longer in the region of lower head and inlet plenum; then, they match the axial nodalization of the core; and then, the nodes representing the upper plenum and upper head are again longer than the core channels. This is done to ensure that each axial node of the reactor vessel sees only one node of the RCCS. The green area above the core is a heat structure representing the thermal shielding for the upper vessel head. The blue cylinders inside the core region represent the heater rod heat structures. For details on each component within the model, readers are referred to reference [15]. The reference model was modified to include just the core, vessel, and RCCS and to provide inlet temperature and flow rate boundary conditions with an outlet pressure boundary condition. Additionally, the thermal conductivity used in the reference model was based on a curve-fit to extrapolate the measured block thermal conductivity,

whereas the model in this work used the block thermal conductivity reported in the facility description without extrapolation. Initial and boundary conditions for the model can be seen in Table 2. The locations of the active heater rods in the experiment straddle the middle and outer rings in the model, so heat is generated in those rings, with nearly 90% of the heat being generated in the outer ring of the core.

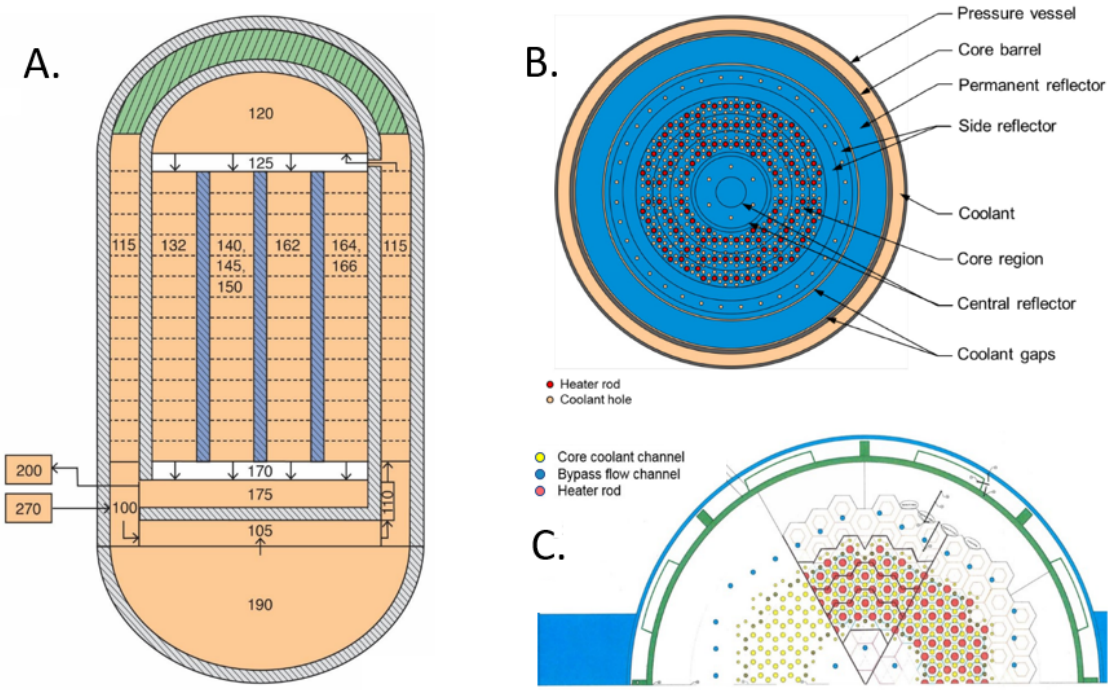

Figure 3. (**A**) Axial nodalization of the RELAP5-3D Model of HTTF (nodalization numbering scheme is described in detail in [15]). (**B**) Radial nodalization of the RELAP5-3D model of HTTF. (**C**) Ring boundary visualization for the core region.

Table 2. PG-27 RELAP5-3D model initial conditions.

Parameter	Value
Helium inlet temperature (°C)	107
Helium pressure (kPa)	130
Helium flow rate (kg/s)	0.1
RCCS inlet temperature (°C)	40
RCCS water pressure (kPa)	100
RCCS flow rate (kg/s)	0.33
RCCS cavity temperature (°C)	27
RCCS cavity air flow rate (g/s)	25
Power (kW)	86.0

The conditions in Table 2 were used for a steady-state run in RELAP5-3D before modeling the PCC portion of the experiment. A simplified power curve was derived from the experimental data and fed into the RELAP5-3D model. The power over time used in the model can be seen in Figure 4. The PCC is initiated at t = 0.0 s and is modeled by reducing the flow from 0.1 to 0.0 kg/s linearly over 1.0 s. The outlet pressure boundary condition was held constant, as were the pressure and flow in the RCCS.

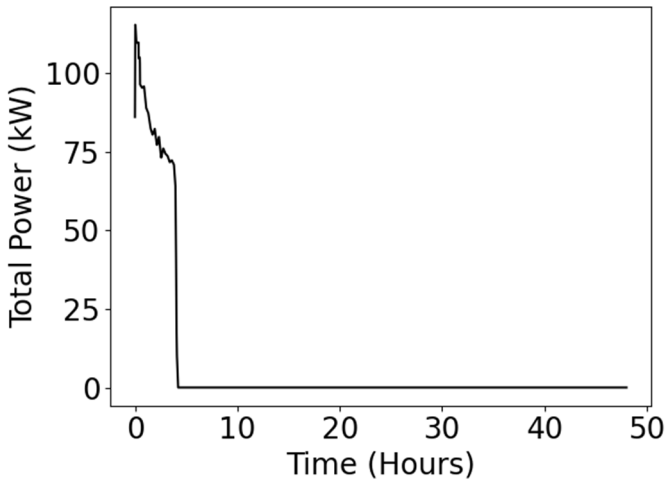

Figure 4. Power versus time in the RELAP5-3D model.

5. CFD Model Development

This study utilized Siemens STAR-CCM+ software, version 2020.1, a versatile commercial CFD tool designed to address various fluid dynamics and heat-transfer challenges by solving the Reynolds-averaged Navier–Stokes (RANS) equations using a finite-volume approach [16]. These equations encapsulate the principles of mass, momentum, and energy conservation in fluid dynamics. The process of Reynolds averaging necessitates employing a turbulence model to account for the turbulent transport of momentum and energy within the flow. A RANS model applies Reynolds decomposition, where an instantaneous quantity is decomposed into its time-averaged and fluctuating quantities. The mean flow and the effects of turbulence on mean flow properties are of interest. Compared to large eddy simulations or direct numerical simulations, the computing resources required for reasonably accurate RANS flow computations are modest, so this approach has been the mainstay of calculating flow phenomena in large, complicated computing domains, such as a nuclear reactor core [4]. The analyzed model accounts for the fluid–solid conjugate heat transfer and resolves the energy conservation equation within solid computational domain structures.

The solution is verified through the following:

(a) Residuals convergence monitoring (residual level of 10^{-4});
(b) Quantities of interest convergence monitoring (solution field no longer changes from iteration to iteration): temperatures and velocities (upper plenum, lower plenum, and coolant channels domains), and heater rods maximum temperature;
(c) Grid convergence index study.

5.1. Geometry

The three-dimensional, full-scale geometry represents one-sixth of the HTTF core blocks; upper, lower, and side reflectors; and lower and upper plenum (Figure 5). The upper plenum volume includes seven instrumentation guide tubes, core volume accounts for 94 core coolant and bypass channels tubes, and the lower plenum domain includes 34 support posts. Total model volume equals 1.25 m^3 (fluid/helium volume ~0.32 m^3).

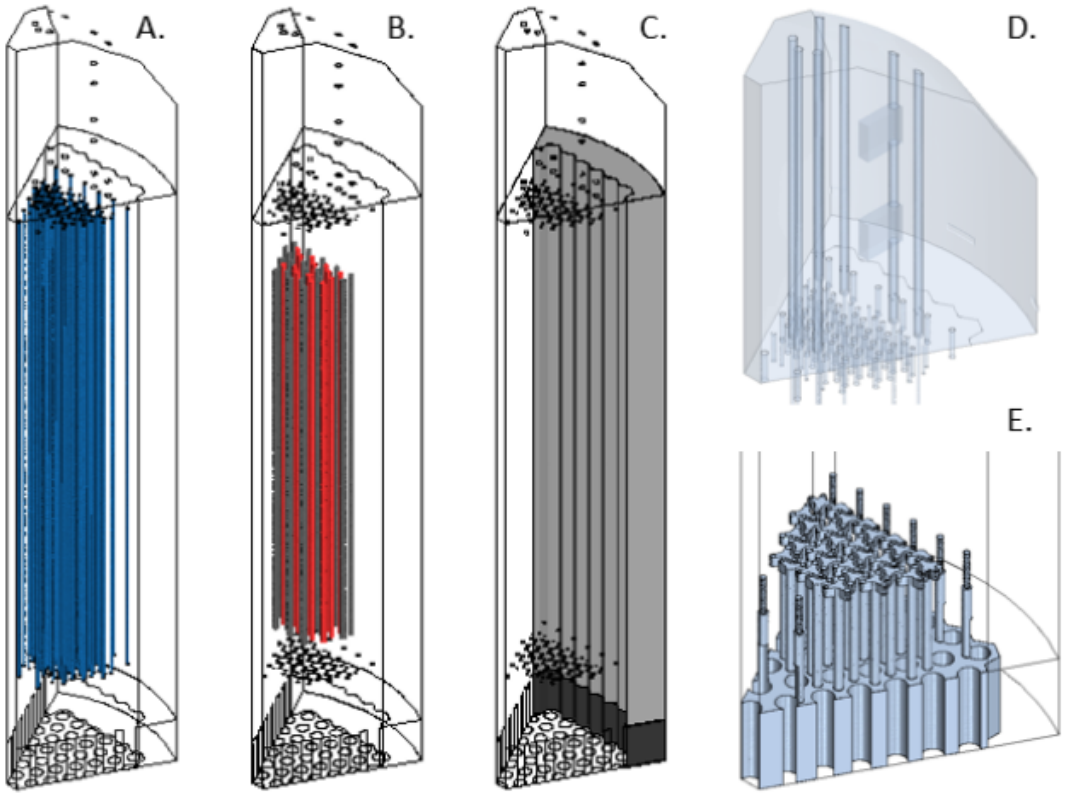

Figure 5. CFD solid and fluid domains: (**A**) coolant channels; (**B**) heating rods (red—operating, black—not used during the test); (**C**) upper and lower side reflectors; (**D**) upper plenum; (**E**) lower plenum with coolant channel transitions.

5.2. Simulation Setup

CFD simulations were carried out as the steady-state calculation and boundary conditions were derived from the RELAP5-3D model results. Transient CFD PCC simulations are impractical due to the analyzed domain's relative size in conjunction with the extended period of the transient [17]. Transient CFD simulations are designed to capture the time-dependent behavior of fluid flows, including unsteady phenomena such as vortex shedding, pulsations, oscillations, and transient heat transfer. When transient calculations are not performed, any time-dependent effects—such as fluctuations, temporal changes in flow patterns, or dynamic interactions—are not represented. In contrast, steady-state simulations operate under the assumption that the flow has reached a condition where variables such as velocity, pressure, and temperature remain constant over time. This approach is suitable for systems that naturally evolve to a steady state or where transient behaviors are minimal or negligible over the period of interest.

For this simulation, the steady-state assumption is considered appropriate because, in the RELAP model, the properties of interest—specifically helium velocity and temperature—have stabilized and do not show significant variation. This assumption is further supported by the findings presented by Bayless (2018). In that study, the HTTF PCC case was run under full power conditions for 168 h following the PCC initiation, adhering to the scaled ANS decay power curve. The results indicated that once reversed flow was achieved, the velocity stabilized and temperature changes were minimal, ranging between 0.5 °C to 1 °C per hour.

Based on this evidence, the steady-state assumption is deemed suitable for the current simulation.

The CFD steady-state simulation refers to a point in time when channel velocity stabilizes, according to RELAP5-3D results. Looking at Figure 6 (where the sign convention is positive upwards), the inner and outer heated core rings' flow reverses about 5.5 h after

transient initiation, followed closely by the flow reversal in the inner reflector (6.5 h). The flow in the middle-heated core ring and side reflector remain in upflow and downflow conditions, respectively, throughout the simulation. The flow reaches quasi-steady-state conditions at ~24 h into the RELAP5-3D transient simulation.

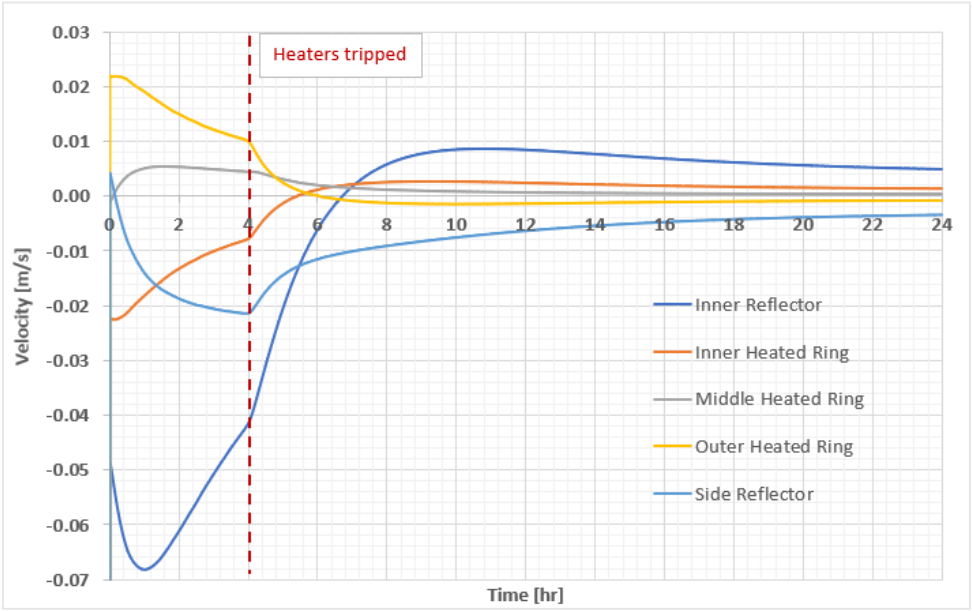

Figure 6. RELAP5-3D PG-27 velocity results.

Todreas et al. [18] described heat-transfer boundary conditions for multiple heated channels connected only at plena. For the zero-net inlet mass flow rate, which physically represents an isolated reactor vessel and relates to the PCC RPV flow conditions, heat extraction or addition from the plena should be specified. For this reason, the upper plenum shroud wall temperature was set to 186.5 °C (based on RELAP5-3D results). The lower plenum is well insulated from the bottom (with a ceramic lower plenum floor, 3.2 cm of structural insulation, and a metallic core support structure); thus, the heat is transferred through the permanent side reflector wall. The permanent side reflector outer wall and upper plenum shroud wall temperature boundary conditions were estimated based on the PG-27 test thermocouple readings. The core, heaters, and coolant temperature initial profiles were extracted from the RELAP5-3D model at the time of flow stabilization (~24 h) and are given in Table 3. Heaters that were used during the PG-27 heat-up phase (heaters 21, 22, 23, 25, 26, 27, and 28; shown in Figure 7) were assigned a static temperature boundary condition with a temperature value of 284.5 °C. Each side of the one-sixth core section was set as a symmetry boundary. The symmetry boundary condition is applicable due to hexagonal symmetry of the reactor pressure vessel and because of the symmetrical heaters' power profile during the PG-27. Table 3 summarizes reference conditions and material properties for the CFD analyses.

The temperatures in this scenario are high enough to generate thermal radiation transfer processes between the hot gas and system walls. Gray thermal radiation with a surface-to-surface radiation model is enabled (with an effective radiation temperature of the environment of 25 °C). The coupled heat transfer between a fluid and an adjoining solid region is also enabled via a solid–fluid interface with zero contact resistance (conjugate heat-transfer model).

Turbulence was calculated with the K-Omega SST (Menter) model. Zhang et al. [19] evaluated that the SST K-Omega model provides accurate results in strong buoyant flow scenarios without significantly increasing the computing time.

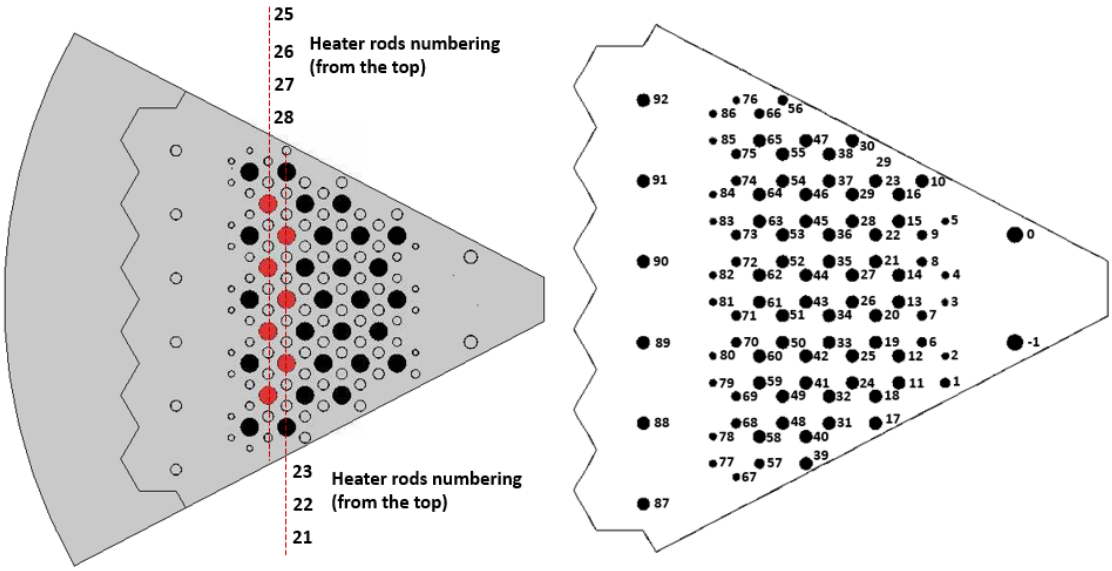

Figure 7. Graphite rods distribution with the rods used during PG-27 test (**left**) and numbering scheme of coolant channels (**right**).

Table 3. CFD model parameters.

Initial and Boundary Conditions					**Source**
Side reflector, outer wall	T = 251.82 °C				PG-27 Test
Upper plenum shroud wall	T = 186.5 °C				PG-27 Test
Upper plenum emissivity	0.072				PG-27 Test & RELAP
System pressure (gauge)	103,675 Pa				PG-27 Test & RELAP
Heaters 21, 22, 23, 24, 25, 26, 27, and 28 axial initial temperature	T = 311.5 °C				RELAP
Radial core temperature	R [m]	Data [°C]			RELAP
	0.124	279.33			
	0.2895	275.25			
	0.377	272.98			
	0.4955	270.64			
	0.6435	265.56			
Radial heaters temperature (profile)	R [m]	Data [°C]			RELAP
	0.2895	290.67			
	0.4955	287.95			
	0.6435	284.81			
Helium axial temperature (profile)	X [m]	Y [m]	Z [m]	Data [°C]	RELAP
	0	0	0	233.5	
	0	0	0.22	276.5	
	0	0	1.8	276.5	
	0	0	4.06	186.5	
Initial velocity	[0,0,0] m/s				N/A

Table 3. *Cont.*

Materials/Gases	
Fluid	Helium [1], compressible, ideal gas
Core, lower plenum posts	Greencast 94-F [2]
Side reflector (core level)	ShotTech SiC 80 [2]
Side reflector (lower plenum level)	Greencast 94-F [2]
Heater rods	Graphite G-348 [3]

[1] Properties taken from the NIST chemistry WebBook; [2] properties taken from Woods [1]; [3] properties taken from McEligot [20].

5.3. Mesh Sensitivity Analysis

The accuracy of the solution heavily depends on the computational grid. The grid size is often constrained by the computational resources available, including memory, processing power, and software licenses. A finer mesh, while more accurate, demands greater resources and extended computation time to achieve a converged solution. Therefore, grid density represents a compromise between precision and the limitations of computational capability.

For this study, an unstructured polyhedral mesh was selected due to its superior ability to model recirculating flows, which are critical in analyzing flow distribution involving natural convection. This fully unstructured meshing approach enables the CFD code to handle complex geometries, such as the HTTF RPV. To accurately capture the boundary layer effects, a prism layer mesh was incorporated. The K-Omega SST turbulence model requires that the near-wall grid be sufficiently refined to maintain a dimensionless wall distance (y+) below one [8,19]. This requirement was met using the All+ Wall treatment model, with five prism layers, a total prism layer thickness of 1.0 mm, and growth and stretching ratios set at 1.5 and 1.3, respectively.

Mesh independence was verified by comparing simulation results across different mesh densities and observing the velocity profile along a probe line in the upper plenum. The grid convergence index (GCI) was computed using a fixed-point iteration method, as specified in the ASME V&V 20-2009 Standard [7]. The GCI quantifies the uncertainty, providing a measure of how close the numerical solution is to the asymptotic value.

The initial coarse mesh number of cells and corresponding mesh base size were selected based on CFD calculations performed by Sato et al. [21] and Tung et al. [10]. Sato et al. [17] analyzed natural circulation flow patterns in the one-twelfth VHTR RPV section using STAR-CCM+ and a total number of 7.6 million cells. For similar geometries (one-twelfth VHTR), Tung et al. [10] applied 11.1 million cells. While the HTTF is scaled as 1:4 in terms of dimensions with reference to the MHTGR, a considerably smaller number of cells could be potentially applied. Nevertheless, aiming at capturing geometrical details and flow behavior at low velocities, the number of cells was kept significantly larger than in the similar simulation work carried out by other researchers in the field, and ultimately, three sets of grids, with 13.74, 21.22, and 32.92 million cells, respectively (Coarse, Medium, and Fine in Table 4), were investigated in the GCI study.

Table 4. Details of the mesh refinement study.

	Coarse	Medium	Fine
# Cells Fluid [million]	13.74	21.22	32.92
# Cells Solid [million]	4.45	4.45	4.45
Total Volume Difference (CAD-Meshed Volume) [m^3]	−0.00132	−0.00192	−0.00252
Characteristic Size Fluid [m]	0.11	0.009	0.007
Characteristic Size Solid [m]	0.014	0.014	0.014

Table 4. *Cont.*

	Coarse	Medium	Fine
Refinement	-	1.15	1.16
Average GCI [%]	-	11.42	6.38
Max Error [m/s]	-	0.13	0.05
Average Error [m/s]	-	0.023	0.011

Figure 8 plots the probe line velocity profiles and GCI index (in the form of uncertainty bands). GCI values for the medium and fine meshes are summarized in Table 4. Figure 9 presents the mesh resolution for the analyzed refinements. Velocity data from three distinct mesh configurations reveal that systematic refinement and finer mesh resolutions yield more precise outcomes. It is crucial to note that local values of computed variables, such as velocity, may not always display smooth or monotonic trends with increasing grid resolution; instead, integral or averaged quantities tend to show more consistent behavior. Observing similar velocity profiles and an average discrepancy of just 0.01 m/s between medium and fine meshes indicates that the refinement process has achieved a satisfactory level of accuracy. Moreover, average domain temperatures were investigated for different discretizations. The average upper plenum and lower plenum temperatures for the medium mesh case were 215 °C and 267 °C, respectively. This translates to an average relative error between fine and medium meshes of 1.2% (upper plenum) and 1.1% (lower plenum).

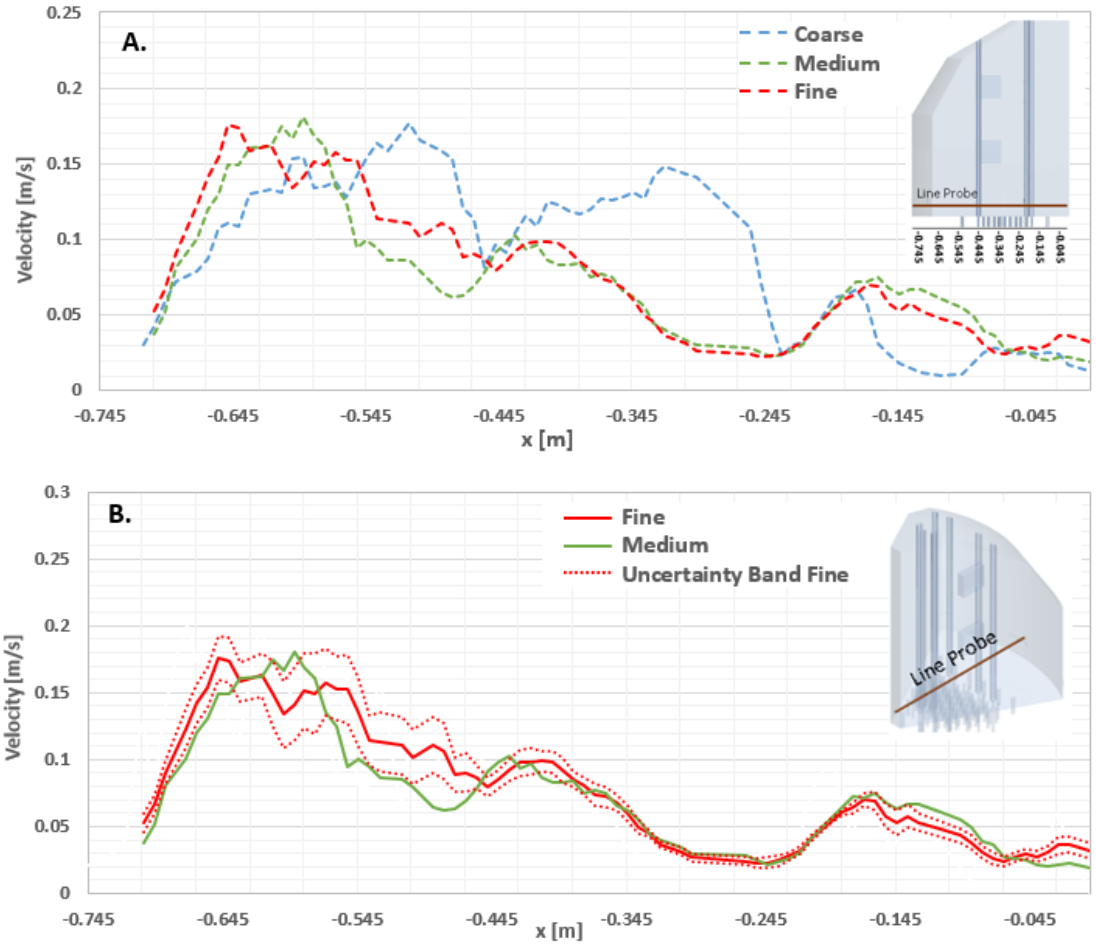

Figure 8. (**A**) Velocity profile along the probe line for coarse, medium, and fine meshes; (**B**) uncertainty bands for fine solution.

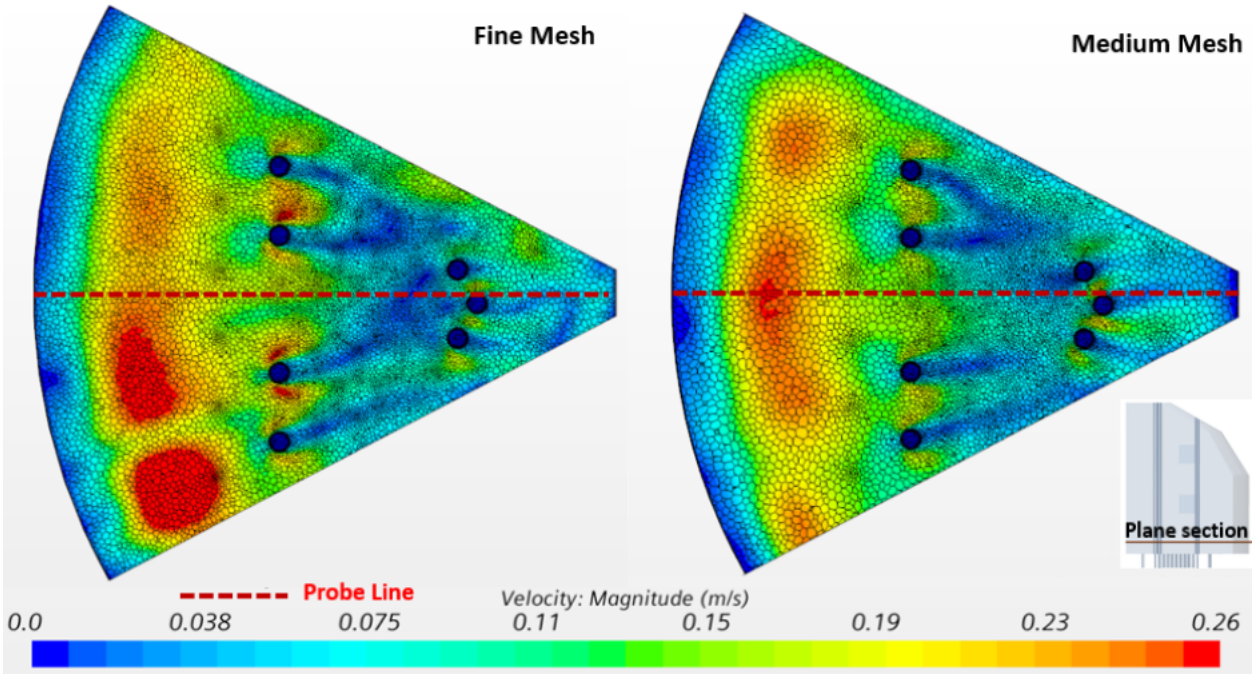

Figure 9. Mesh and velocity distribution at Plane Section 1 for the medium and fine discretization.

While the velocity profile from the medium mesh does not perfectly align with the fine mesh results, given the preliminary nature of the analysis, an average Grid Convergence Index (GCI) of 8.4% for the medium mesh was deemed acceptable. This compromise enables the generation of reasonably high-quality data while conserving computational resources and time. The computing setup utilized included 96 parallel CPUs and 384 GB of RAM, with a total wall-clock simulation time of 505 h for the medium mesh scenario.

6. Results

The PCC intracore natural circulation flow map is presented in Figure 10. The natural circulation velocity is higher for the channels located in the outer core ring. In general, channels closer to the core center exhibit upflow (29 channels total) (Figure 11B), while those near side reflectors are in downflow (65 channels). Average axial downflow and upflow velocities are –0.002 and 0.0015 m/s, respectively. The Rayleigh number, calculated as the product of the Grashof number (which characterizes the interplay between buoyancy forces and viscosity) and the Prandtl number (which indicates the ratio of momentum diffusivity to thermal diffusivity), for the coolant channels is approximately 2.6×10^8. This value suggests that the flow regime is turbulent in nature [22].

The obtained flow pattern differs from the map presented by Gutowska et al. in 2018 [13]. In the previous work, a different power input (total core power input of 37 kW, 37.5 h from the beginning of the transient) was applied to a larger number of heater rods along with higher temperature boundary conditions. These conditions were based on the anticipated nominal HTTF operating conditions during the loss-of-flow experiment and were supported by the pretest RELAP5-3D calculations given in [15,23]. Similarly to the results in this paper, channels closer to the core center exhibited upflow (total of 31 channels) while those near side reflectors were in downflow (63 channels). Average axial velocities were higher than in the current work: Downflow and upflow velocities were equal to −0.03 and 0.02 m/s, respectively, and the Rayleigh number was $3.5–4.0 \times 10^9$. The differences between the previous work by Gutowska et al. in 2018 [13] and this work are likely the result of different power input stemming from differences between planned and actual test conditions.

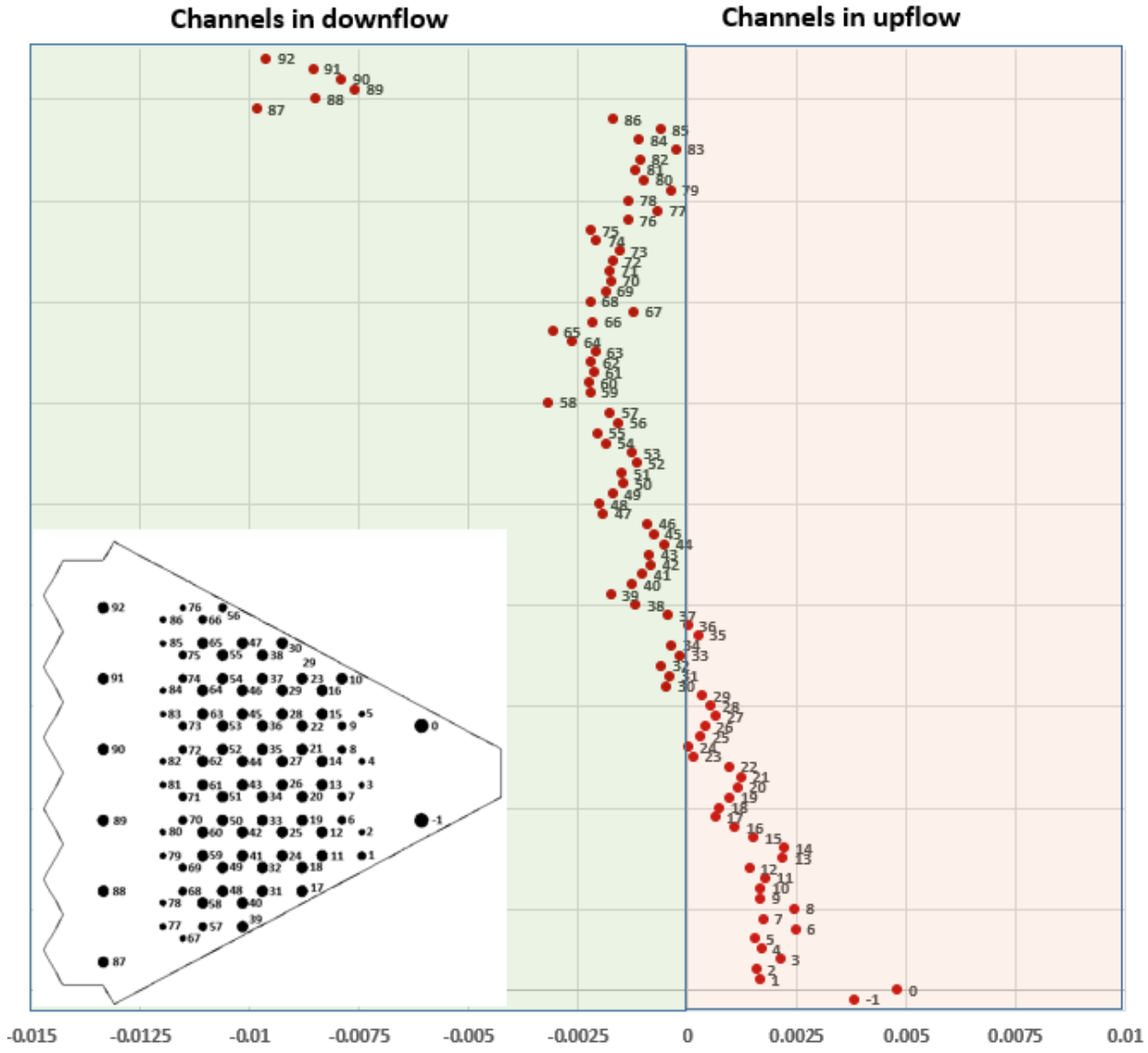

Figure 10. Intracore natural circulation flow velocity map [m/s] 24 h from the beginning of the PCC transient.

Table 5 lists the average axial velocities in the HTTF coolant channels obtained from RELAP5-3D and STAR-CCM+. Average velocities in the respective rings present the same flow direction in respective channel groups and are of a similar value and the same order of magnitude. Differences in the average velocity values might result from the following:

1. CFD model
   - Uncertainty associated with the CFD boundary conditions (constant temperatures at the upper plenum and side reflector outer walls); further refinement of the CFD model boundary conditions could impact the temperature difference between the upper and lower plenum and ultimately the channels velocity but should not significantly change the flow map;
   - Further mesh refinement to achieve lower GCI values (at the cost of increased computing power needs).
2. RELAP5-3D model
   - System codes do not provide details on the three-dimensional flow distribution, and information about the localized flow phenomena is not available;

- The employed RELAP5-3D model nodalization coarsely groups coolant channels into five rings, losing details of the flow in single channels;
- RELAP5-3D calculates the natural convection Nusselt number using the Churchill–Chu correlation, which was developed for the free convection regime in vertical parallel plates [24] (the analyzed geometry comprises multiple elongated vertical channels of a high aspect ratio): Channel's heat transfer and ultimately density and velocity distribution could be affected by this correlation application.

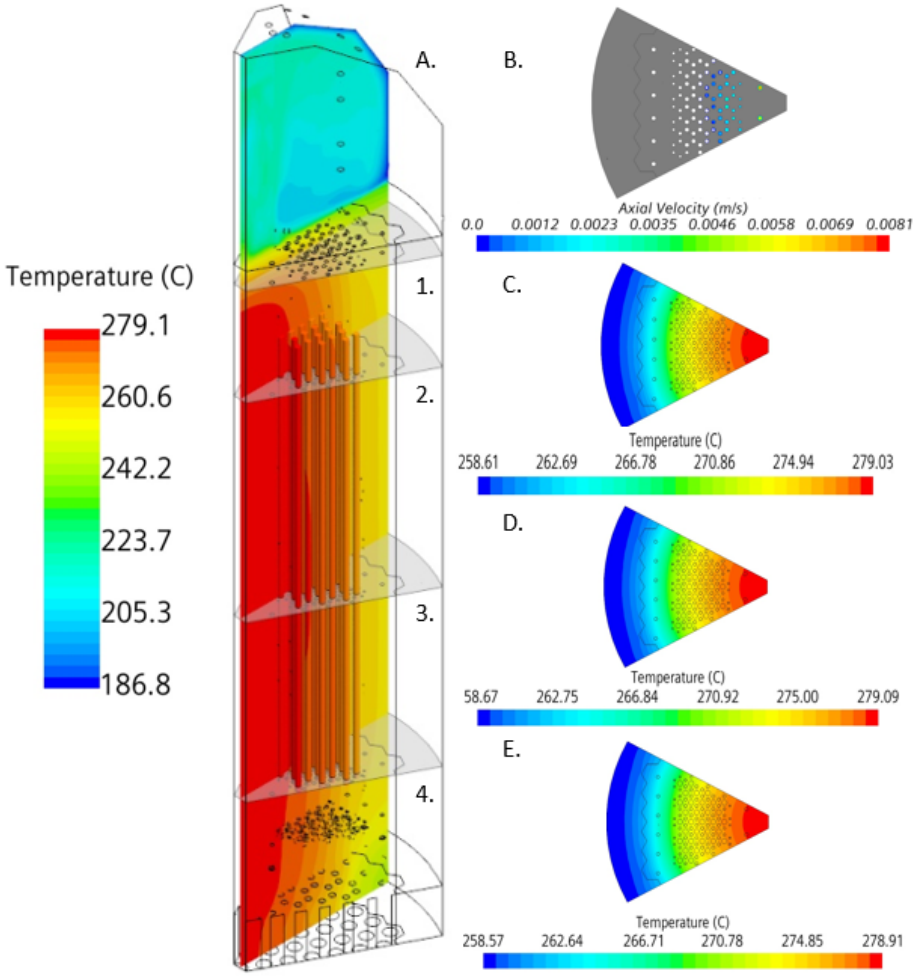

Figure 11. (**A**) Vertical temperature distribution in the core; (**B**) channels in upflow, with reference to cross-section 1; (**C**–**E**) horizontal temperature distribution at cross-sections 2, 3, and 4, respectively.

With the heat removal being primarily in the radial direction, the highest temperatures will be in the middle of the vessel, with the temperatures decreasing as the distance from the center of the vessel increases. The core temperature distribution is shown in Figure 11A,C–E.

According to the RELAP5-3D model, the maximum temperature of heater rods was in the inner ring at 295.2 °C. The CFD results provide a maximum temperature ~17.8 °C lower than the RELAP5-3D predictions. The difference in temperatures between RELAP5-3D and STAR-CCM+ most likely occurs because of the constant temperature boundary condition application in the CFD model.

From the CFD results, the upper and lower plenums' average temperatures are 267.3 °C and 215 °C, respectively. The RELAP5-3D analysis gives 233.7 °C for the lower plenum and ~186 °C for the upper plenum volumes. The difference of 33.5 °C in the average lower plenum temperatures might stem from the fact that the CFD lower plenum

volume includes coolant channel volumes up to the channel transitions (located in the lower reflector). The difference of 29 °C in the average upper plenum temperatures is likely due to the constant upper plenum shroud wall temperature boundary condition that does not reflect the shroud temperature profile. It was impossible to provide a better estimation of the shroud temperature profile based on the limited thermocouples installed at this location. The helium temperature rise from the lower to the upper plenum is 52 °C in STAR-CCM+ and 48 °C in RELAP5-3D. This difference may arise from differences in the heat-transfer coefficient between RELAP5-3D and STAR-CCM+ because the velocities in STAR-CCM+ are slightly higher than in RELAP5-3D, leading to less heat deposited in the helium, or a combination of both factors. It should also be noted that the RELAP5-3D model is a transient model with temperatures changing over time, whereas the STAR-CCM+ model is a steady-state model with derivatives overtime set to zero.

Table 5. Comparison of axial average velocities in the HTTF core channels between RELAP5-3D and STAR-CCM+.

	# of Channels in the RELAP5-3D (Full Core)	Corresponding STAR-CCM+ Channels (One-Sixth Section)	STAR-CCM+	RELAP5-3D	Difference (m/s, STAR-CCM+ - RELAP5-3D)	Relative Difference (Difference/ STARCCM+)
Inner reflector	6	−1–0	0.0043 m/s	0.0035 m/s	0.0008 m/s	18.6%
Inner heated ring	138	1–23	0.0015 m/s	0.0007 m/s	0.0008 m/s	53.3%
Middle heated ring	144	24–47	−0.00044 m/s	−0.00040 m/s	−0.00004 m/s	9.1%
Outer heated ring	234	48–86	−0.0017 m/s	−0.0014 m/s	−0.0003 m/s	17.6%
Side reflector	36	87–92	−0.0086 m/s	−0.0050 m/s	−0.0036 m/s	41.9%

The flow field inside the upper plenum is presented in Figure 12A. Localized asymmetry in the flow field is caused by unevenly distributed instrumentation tubes and gas capacitance sensors. After helium enters the upper plenum volume through channels in upflow, flow streams collide at the center and propagate sideways. Before helium exits the plenum toward channels that are in a downflow, the recirculation zone is created between the center stream and colder plenum head side walls. The described flow pattern is not present in the lower plenum volume. Densely packed support posts disturb the recirculating flow pattern (Figure 12B).

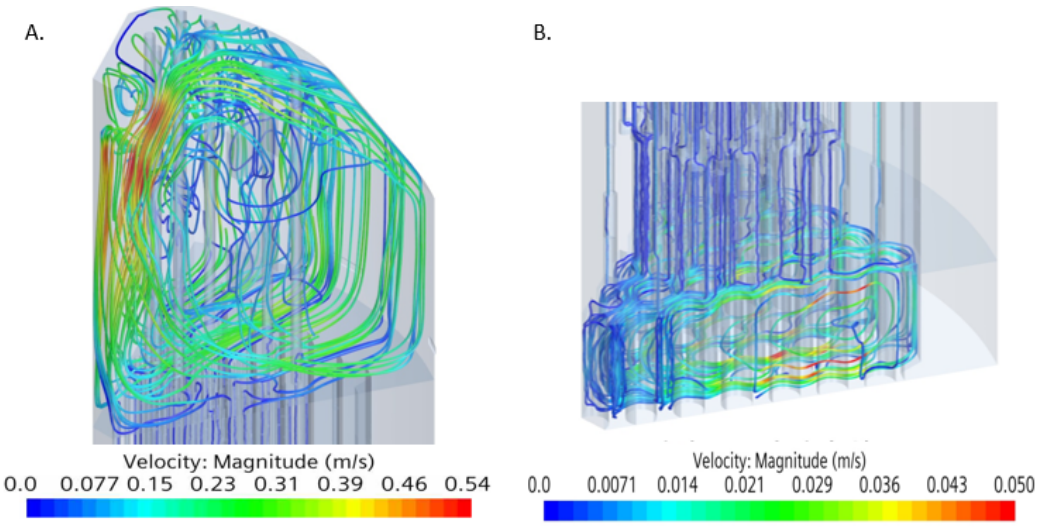

Figure 12. (**A**) Velocity streamlines in the upper plenum; (**B**) velocity streamlines in the lower plenum.

7. Conclusions and Future Work

The results from the CFD simulations offer comprehensive insights into the distribution of helium during the natural circulation within the core that occurs after the PCC transient. This analysis serves as a foundational reference for future sensitivity assessments and code validation efforts. It establishes a baseline that allows for the comparison of how variations in temperature profiles, turbulence modeling approaches, and other relevant parameters impact the system, facilitating the assessment of sensitivities. The outcomes of the CFD simulations enhance understanding of local flow behavior and mixing within the HTTF RPV structures. System characteristics, particularly regarding the flow capacity of specific channels, can be used to calculate similarity groups between the prototype and reference reactor designs. Proceeding with similarity group calculations requires data on the reference MHTGR intracore natural circulation patterns. With numerical results for both the test and prototype facilities, it becomes possible to assess how closely the PG-27 experiment reproduces the physics of the full-scale installation it aims to represent.

Future work will also focus on further refining and validating the RELAP model. Once validation is complete, additional CFD simulations will be conducted using data from the validated system model. Currently, the CFD conditions used in this study are based on an available, published RELAP model that has not yet undergone full validation. Preliminary comparisons show good agreement in the upper plenum temperatures (approximately 230 °C for the lower thermocouples and 220 °C for the upper thermocouples), although the lower plenum and core temperatures observed in the experiment are significantly higher by about 100 °C.

The methodology outlined in this paper demonstrates the approach to intracore natural circulation modeling in STAR-CCM+ and describes the necessary model inputs based on realistic experimental conditions. Once improved boundary conditions are available, the model setup can be replicated using this verified approach to generate results that can be further utilized for CFD validation. Additionally, future CFD studies will include analyses of the 1/6th section of the MHTGR RPV, with boundary and initial conditions scaled up from the HTTF numerical model.

Author Contributions: Conceptualization, I.G.; methodology, I.G.; Star CCM+ simulations, I.G.; investigation, I.G.; RELAP5-3D analysis, R.K.; Data curation, I.G. and R.K.; writing—original draft preparation, I.G. and R.K.; review and editing, I.G., R.K., B.G.W. and N.R.B.; supervision, B.G.W. and N.R.B. All authors have read and agreed to the published version of the manuscript.

Funding: This research received no external funding.

Data Availability Statement: Dataset available on request from the authors.

Acknowledgments: This manuscript has been authored by Battelle Energy Alliance, LLC under Contract No. DE-AC07-05ID14517 with the U.S. Department of Energy. The U.S. Government retains and the publisher, by accepting the article for publication, acknowledges that the U.S. Government retains a nonexclusive, paid-up, irrevocable world-wide license to publish or reproduce the published form of this manuscript or allow others to do so for U.S. Government purposes.

Conflicts of Interest: The authors declare no conflict of interest.

Abbreviations

ASME	American Society of Mechanical Engineers
CAD	Computer-Aided Design
CFD	Computational Fluid Dynamics
DCC	Depressurized Conduction Cooldown
GCI	Grid Convergence Index
HTTF	High Temperature Test Facility
MHTGR	Modular High-Temperature Gas-cooled Reactor
NIST	National Institute of Standards and Technology
PCC	Pressurized Conduction Cooldown

RANS	Reynolds-averaged Navier–Stokes
RCCS	Reactor Cavity Cooling System
RPV	Reactor Pressure Vessel
VHTR	Very-High-Temperature Reactor
V&V	Verification and Validation

References

1. Woods, B. OSU High Temperature Test Facility Design Technical Report, Revision 2. United States. 2019. Available online: https://www.osti.gov/servlets/purl/1599410 (accessed on 1 November 2024).
2. Ball, S.J.; Fisher, S.E. *Next Generation Nuclear Plant Phenomena Identification and Ranking Tables (PIRTs)*; NUREG/CR-6944; Nuclear Regulatory Commission: Rockville, MD, USA, 2008.
3. Oh, C.H.; Davis, C.; Siefken, L.; Moore, R.; No, H.C.; Kim, J.; Park, G.C.; Lee, J.C.; Martin, W.R. *Development of Safety Analysis Codes and Experimental Validation from a Very High Temperature Gas Cooled Reactor*; INL/EXT-06-01362; Idaho National Laboratory: Idaho Falls, ID, USA, 2006.
4. Versteeg, H.K.; Malalasekera, W. *An Introduction to Computational Fluid Dynamics: The Finite Volume Method*; Longman Scientific and Technical: Harlow, UK, 1995.
5. MacDonald, P.E. *Next Generation Nuclear Plant Research and Development Program Plan*; INEEL/EXT-05-02581; INL: Hong Kong, China, 2005.
6. Vilim, R.B.; Pointer, W.D.; Wei, T.Y.C. *Prioritization of VHTR System Modeling Needs Based on Phenomena Identification, Ranking and Sensitivity Studies*; ANL-GenIV-071; Argonne National Laboratory: Lemont, IL, USA, 2006.
7. *V&V 20-2009*; Standard for Verification and Validation in Computational Fluid Dynamics and Heat Transfer. American Society of Mechanical Engineers: New York, NY, USA, 2009.
8. Tung, Y.; Johnson, R.W.; Ferng, Y.; Chieng, C. Modeling Strategies to Compute Natural Circulation Using CFD in a VHTR After a LOFA. *Nucl. Eng. Des.* **2014**, *275*, 80–90. [CrossRef]
9. Oh, C.H.; Kim, E.S.; Kang, H.S. Natural Circulation Patterns in the VHTR Air-ingress Accident and Related Issues. *Nucl. Eng. Des.* **2012**, *249*, 228–236. [CrossRef]
10. Tung, Y.; Johnson, R.W. CFD Calculations of Natural Circulation in a High Temperature Gas Reactor Following Pressurized Circulator Shutdown. *ASME Int. Mech. Eng. Congr. Expo.* **2011**, *10*, 1169–1177.
11. Hassan, Y. *Investigation on the Core Bypass Flow in a Very High Temperature Reactor*; NEUP Project No. 09-840; Nuclear Energy University Program: Washington, DC, USA, 2013.
12. Alwafi, A.; Nguyen, T.; Hassan, Y.; Anand, N. Time-resolved Particle Image Velocimetry Measurements of a Single Impinging Jet in the Upper Plenum of a Scaled Facility of High Temperature Gas-cooled Reactors. *Int. J. Heat Fluid Flow* **2019**, *76*, 113–129. [CrossRef]
13. Gutowska, I.; Woods, B.G. CFD assessment of LOFA intra core natural circulation in the High Temperature Test Facility. In Proceedings of the NURETH-18, Portland, OR, USA, 18–23 August 2018.
14. Woods, B.G. *Scaling Analysis for the Very High Temperature Reactor Test Facility at Oregon State University*; Technical Report, OSU-HTTF-TECH-001-R0; Oregon State University: Corvallis, OR, USA, 2015.
15. Bayless, P.D. *RELAP5-3D Input Model for the High Temperature Test Facility*; INL/EXT-18-45579; Idaho National Laboratory: Idaho Falls, ID, USA, 2018.
16. CD-adapco. *Starccm+ Documentation*; Version 10.06; CD-adapco: Melville, NU, USA, 2015.
17. Boyd, C.; Armstrong, K. *Computational Fluid Dynamics Analysis of Natural Circulation Flows in a Pressurized-Water Reactor Loop under Severe Accident Conditions*; NUREG-1922; U.S. Nuclear Regulatory Commission: Rockville, MD, USA, 2010.
18. Todreas, N.E.; Kazimi, M.S. *Nuclear Systems II, Elements of Thermalhydraulic Design*; Hemisphere Publishing Corporation: London, UK, 1990.
19. Zhang, Z.; Zhang, W.; Zhai, Z.; Chen, Q. Evaluation of Various Turbulence Models in Predicting Airflow and Turbulence in Enclosed Environments by CFD: Part-2: Comparison with Experimental Data From Literature. *HVACR Res.* **2017**, *13*, 871–886. [CrossRef]
20. McEligot, D.; Swank, W.D.; Cottle, D.L.; Valentin, F.I. *Thermal Properties of G-348 Graphite*; Idaho National Laboratory (INL): Idaho Falls, ID, USA, 2016.
21. Sato, H.; Johnson, R.W.; Schultz, R.R. Computational Fluid Dynamic Analysis of Core Bypass Flow Phenomena in a Prismatic VHTR. *Ann. Nucl. Energy* **2010**, *37*, 1172–1185. [CrossRef]
22. Çengel, Y.A. *Heat Transfer: A Practical Approach*, 2nd ed.; McGraw-Hill: New York, NY, USA, 2004.
23. Bayless, P.D. *RELAP-3D Pre-test Prediction for High Temperature Test Facility Test PG-26*; INL/EXT-18-45717; Idaho National Laboratory: Idaho Falls, ID, USA, 2018.
24. Churchill, S.W. *Heat Exchanger Design Handbook*; Hemisphere: Washington, DC, USA, 1983.